

Entanglement in dual unitary quantum circuits with impurities

Shachar Fraenkel¹ and Colin Rylands²

¹*Raymond and Beverly Sackler School of Physics and Astronomy, Tel Aviv University, Tel Aviv 6997801, Israel*

²*SISSA and INFN Sezione di Trieste, via Bonomea 265, 34136 Trieste, Italy*

Bipartite entanglement entropy is one of the most useful characterizations of universal properties in a many-body quantum system. Far from equilibrium, there exist two highly effective theories describing its dynamics – the quasiparticle and membrane pictures. In this work we investigate entanglement dynamics, and these two complementary approaches, in a quantum circuit model perturbed by an impurity. In particular, we consider a dual unitary quantum circuit containing a spatially fixed, non-dual-unitary impurity gate, allowing for differing local Hilbert space dimensions to either side. We compute the entanglement entropy for both a semi-infinite and a finite subsystem within a finite distance of the impurity, comparing exact results to predictions of the effective theories. We find that for a semi-infinite subsystem, both theories agree with each other and the exact calculation. For a finite subsystem, however, both theories qualitatively differ, with the quasiparticle picture predicting a non-monotonic growth in contrast to the membrane picture. We show that such non-monotonic behavior can arise even in random chaotic circuits, pointing to a hitherto unknown shortcoming of the membrane picture in describing such systems.

Introduction— One dimensional quantum systems are particularly susceptible to the influence of interactions [1]. A prime example of this is found by coupling such a system to a quantum impurity. This can have a drastic effect not only on the transport of a system [2] but also on its spectral properties. Indeed a single impurity added to an otherwise integrable system can be enough for it to exhibit properties of quantum chaos [3–11]. Despite this, however, the underlying integrability of the pure system can manifest itself in certain settings such as ballistic transport of charge in a non-equilibrium steady state [12]. Quantum impurities thus provide an interesting probe with which to study the behavior of many-body systems, and the interplay with integrability breaking, particularly out of equilibrium.

For a non-equilibrium system, one of the most fundamental and insightful quantities one can calculate is the bipartite entanglement entropy [13]. Two complementary effective theories exist to describe this quantity: the quasiparticle picture [14] and the entanglement membrane picture [15, 16]. In the former, entanglement between spatial regions is created by the propagation of correlated sets of quasiparticles [14]. By calculating how these quasiparticles are correlated initially one can make quantitative predictions on the growth of entanglement. The theory applies to integrable models, free or interacting [17], and has been adapted also to many other scenarios [18–30]. In the latter theory, entanglement does not spread throughout the system via quasiparticles but is instead produced locally and can be computed by studying a membrane in space-time which separates the subsystem from its complement [15, 16]. The only input this requires is the energy or tension associated to the membrane, however this is difficult to determine and has only been achieved in a limited number of cases [16, 31, 32]. In contrast to the quasiparticle picture, the membrane theory applies to chaotic models. For contiguous subsystems both theories provide the same qualitative results, namely the linear growth of entanglement from lowly en-

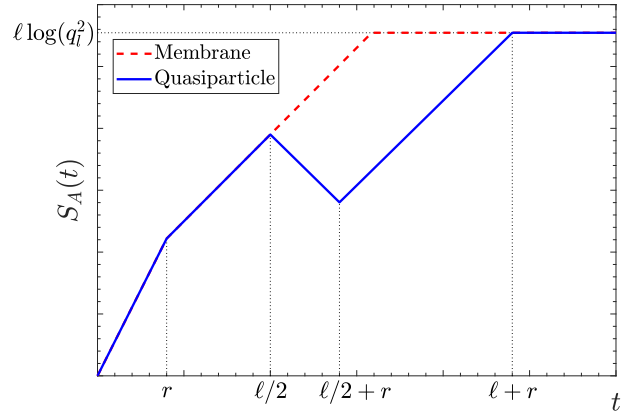


FIG. 1. The dynamics of the entanglement entropy for a dual unitary circuit perturbed by an impurity. Subsystem A has length 2ℓ and is a distance $2r$ from the impurity. The solid blue line is for bulk swap gates with local Hilbert space dimension $q_l = 2$ and the impurity given in (16), with $c = 0.05$, which matches the quasiparticle prediction. The red dashed line represents the prediction of the membrane picture for the same impurity gate but with a generic dual unitary bulk gate.

tangled states, a fact which can be understood using the unifying approach of space-time duality [33]. For finite-size systems or disjoint subsystems, however, the two approaches give qualitatively different predictions [34–37] revealing the distinct properties of the models to which they apply.

An ideal setting in which to study these contrasting approaches is given by dual unitary quantum circuits. These constitute a particular class of many-body quantum systems that describes a wide range of dynamics from integrable to chaotic while at the same time retaining a degree of solubility [38–49]. Many of their properties, including their bipartite entanglement entropy, have

been calculated exactly [50–53], and recently they also provided the first analytic verification of both the membrane and quasiparticle pictures in the case of disjoint intervals [35].

In this work we consider a hybrid system consisting of two dual unitary circuits, with possibly different local Hilbert space dimensions, stitched together via a quantum impurity. The impurity is represented by a line of gates at a fixed position which are not dual unitary. In this setup we calculate the entanglement entropy between a subsystem that does not contain the impurity and its complement, for both semi-infinite and finite subsystems, and compare with the predictions of the quasiparticle and membrane pictures. We find that for a semi-infinite subsystem, the exact calculation can be interpreted using either the quasiparticle or membrane pictures.

For a finite subsystem, however, the two predictions qualitatively differ, see Fig. 1. In particular, after an initial period of linearly growing entanglement, the quasiparticle picture predicts a period of decreasing entanglement entropy followed by a return to growth and an eventual saturation. This is in contrast to the membrane picture, which always predicts monotonic growth before saturation. Indeed, our exact calculation agrees with the quasiparticle picture for an integrable circuit, and with the membrane picture for a maximally-ergodic random circuit. Surprisingly, we find that, in between these two extremes, the non-monotonic behavior appears even for chaotic random circuits, indicating that the membrane picture fails to describe their entanglement dynamics.

Setting— We consider a one dimensional chain of $2L$ qudits with L even, located at coordinates $x = 1, \dots, 2L$. Each qudit has local Hilbert space dimension q_x where $q_{x \leq L} = q_l$ and $q_{x > L} = q_r$. The system is initialized in the state

$$|\Psi(0)\rangle = \bigotimes_{x=1}^L |m_x\rangle, \quad |m_x\rangle = \frac{1}{q_x^{\frac{1}{2}}} \sum_{i,j=1}^{q_x} [m_x]_{ij} |ij\rangle_x, \quad (1)$$

where $|ij\rangle_x = |i\rangle_{2x-1} \otimes |j\rangle_{2x}$ with $|i\rangle_y, i = 1, \dots, q_y$ spanning the set of states of the qudit at site y , and $\{m_x\}$ is a set of $q_{2x} \times q_{2x}$ unitary matrices characterizing the initial state. Such states are the simplest type of solvable initial states for a dual unitary circuit [51]. The dynamics of the system are generated by a brickwork-pattern quantum circuit, such that the state of the system after $t + 1$ time steps is given by

$$|\Psi(t+1)\rangle = \mathbb{U}(t+1) |\Psi(t)\rangle, \quad (2)$$

and where the time-evolution operator is

$$\mathbb{U}(t) = \bigotimes_{x \text{ odd}} U_{x,x+1}(x,t) \bigotimes_{x' \text{ even}} U_{x',x'+1}(x',t). \quad (3)$$

Here $U_{x,x+1}(x,t)$ are unitary operators acting on the whole chain, but non-trivially only at sites $x, x+1$ as $U(x,t)$, and as the identity elsewhere. The $q_x q_{x+1} \times q_x q_{x+1}$ matrices $U(x,t)$ are called local gates, and in

our system we take them to be of one of two different types, a bulk gate or an impurity gate. The bulk gates comprise almost all of the system except for a line of impurity gates located at $x = L, \forall t$. While both types of gates are unitary when viewed in the time-like direction, i.e. $U(x,t)U^\dagger(x,t) = \mathbb{1}, \forall x,t$, the bulk gate is also dual unitary, meaning it is unitary in the space-like direction as well. The local gates thus obey $\tilde{U}(x,t)\tilde{U}^\dagger(x,t) = \mathbb{1}, \forall x \neq L$, where

$$\langle ij | \tilde{U}(x,t) | kl \rangle = \langle j | U(x,t) | ik \rangle. \quad (4)$$

We need not take any of the bulk or impurity gates to be the same, and indeed later on we will examine a system of randomly chosen bulk gates. When $q_l = q_r$, it is possible to take the limit where the impurity gate is also dual unitary and reproduce results for the pure dual unitary circuit. When $q_l \neq q_r$, the impurity can never be made dual unitary.

Our quantity of interest is the Rényi entanglement entropy between a subsystem A and its complement \bar{A} ,

$$S_A^{(n)}(t) = \frac{1}{1-n} \log \text{tr}[\rho_A^n(t)], \quad (5)$$

where $\rho_A(t) = \text{tr}_{\bar{A}}[|\Psi(t)\rangle\langle\Psi(t)|]$ is the reduced density matrix of A . Taking the replica limit, $n \rightarrow 1$, we obtain the von-Neumann entanglement entropy $S_A(t) = \lim_{n \rightarrow 1} S_A^{(n)}(t)$. The subsystem is composed of 2ℓ contiguous sites a distance $2r$ from the impurity, $A = (L - 2\ell - 2r, L - 2r]$.

We may represent our quantum circuit and conveniently perform calculations diagrammatically using the standard graphical notation of tensor networks [54]. Specifically, we represent the folded, replicated local gate as

$$[U(x,t) \otimes U^*(x,t)]^{\otimes_r n} = \begin{array}{c} \text{---} \\ \text{---} \end{array} \text{ or } \begin{array}{c} \text{---} \\ \text{---} \end{array}, \quad (6)$$

$$[U(L,t) \otimes U^*(L,t)]^{\otimes_r n} = \begin{array}{c} \text{---} \\ \text{---} \end{array}, \quad (7)$$

where we have denoted by \otimes_r the tensor product over different replicas. When necessary, we shall distinguish between different local Hilbert space dimensions using thin or thick lines for q_l, q_r , respectively. We also introduce the two special states on the replicated Hilbert space and their corresponding graphical depictions

$$\sum_{s_j \in \mathbb{Z}_{q_x}} |s_1, s_1, s_2, s_2, \dots, s_n, s_n\rangle = \bigcirc, \quad (8)$$

$$\sum_{s_j \in \mathbb{Z}_{q_x}} |s_1, s_2, s_2, s_3, \dots, s_n, s_1\rangle = \square.$$

The first state, represented by the empty circle, couples together the forward and backward time evolution on the same replica, whereas the second state instead couples the backward time evolution in one copy to that of the forward time evolution in the next copy.

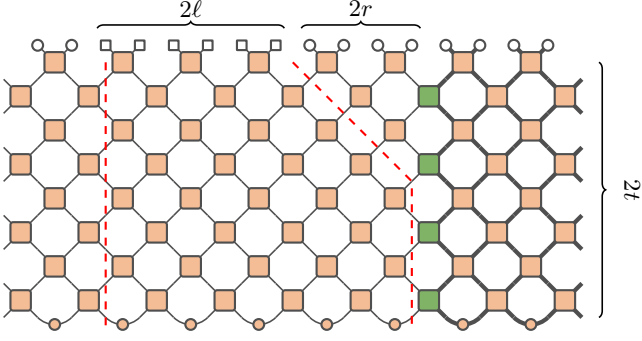


FIG. 2. The diagrammatic representation of $\text{tr}[\rho_A^n(t)]$ with $\ell = 3, r = 2$ and for $t = 4$. Orange boxes denote bulk dual unitary operators while green represents the impurity. The local Hilbert space dimension to the left and right of the impurity is q_l and q_r , respectively. This is depicted using thin and thick lines. The dashed red lines indicate the paths of the entanglement membranes before the entropy saturates.

The unitarity of the local gates is expressed graphically as

$$\begin{array}{c} \square \\ \diagdown \quad \diagup \\ \square \end{array} \circ = \begin{array}{c} \circ \\ \diagdown \quad \diagup \\ \circ \end{array}, \quad \begin{array}{c} \square \\ \diagdown \quad \diagup \\ \square \end{array} \square = \begin{array}{c} \square \\ \diagdown \quad \diagup \\ \square \end{array}, \quad \begin{array}{c} \square \\ \diagdown \quad \diagup \\ \square \end{array} \circ = \begin{array}{c} \circ \\ \diagdown \quad \diagup \\ \circ \end{array}, \quad \begin{array}{c} \square \\ \diagdown \quad \diagup \\ \square \end{array} \square = \begin{array}{c} \square \\ \diagdown \quad \diagup \\ \square \end{array}, \quad (9)$$

along with the same diagrams flipped about the horizontal axis. For the bulk gates, we have the additional dual unitarity conditions

$$\begin{array}{c} \circ \\ \diagdown \quad \diagup \\ \square \end{array} = \begin{array}{c} \circ \\ \diagdown \quad \diagup \\ \circ \end{array}, \quad \begin{array}{c} \square \\ \diagdown \quad \diagup \\ \square \end{array} = \begin{array}{c} \square \\ \diagdown \quad \diagup \\ \square \end{array}, \quad (10)$$

along with the same diagrams flipped about the vertical axis. The replicated initial state is represented as

$$(|m_x\rangle \otimes |m_x\rangle^*)^{\otimes n} = \begin{array}{c} \diagdown \quad \diagup \\ \circ \end{array}, \quad (11)$$

which due to the unitarity of the matrix m_x obeys the following relations:

$$\begin{array}{c} \circ \\ \diagdown \quad \diagup \\ \circ \end{array} = \frac{1}{\circ \circ} \begin{array}{c} \diagdown \quad \diagup \\ \circ \end{array}, \quad \begin{array}{c} \square \\ \diagdown \quad \diagup \\ \square \end{array} = \frac{1}{\square \square} \begin{array}{c} \diagdown \quad \diagup \\ \square \end{array}, \quad (12)$$

along with the same diagrams flipped about the vertical axis. Here the coefficients $\circ \circ = \square \square = q_x^n$ come from the normalization of the initial state. Using this notation we can depict $\text{tr}[\rho_A^n(t)]$ using the diagram in Fig. 2.

Semi-infinite subsystem— We begin with the calculation of the bipartite Rényi entanglement entropy of a semi-infinite subsystem, $\ell = L/2 - r$ and $L \rightarrow \infty$. Our starting point is the diagrammatic representation of $\text{tr}[\rho_A^n(t)]$ shown in Fig. 2. Using the unitarity of the local gates, (9), this can be significantly reduced so that all gates can be removed apart from those forming a backwards light cone emanating from the interface between

A and \bar{A} . The result is that

$$\text{tr}[\rho_A^n(t)] = \begin{array}{c} \diagdown \quad \diagup \\ \begin{array}{c} \square \\ \diagdown \quad \diagup \\ \square \end{array} \\ \diagdown \quad \diagup \\ \begin{array}{c} \circ \\ \diagdown \quad \diagup \\ \circ \end{array} \end{array} \quad 2t, \quad (13)$$

where we have depicted explicitly the case of $t = 4$ and $r = 2$. From this we see that the impurity gate does not appear if $t \leq r$, in which case we recover the pure dual unitary result. The diagram can likewise be reduced when $t > r$, whereupon the impurity gate affects the growth of entanglement. Relying on the property $\square \circ = \circ \square = q_x$, the final result is

$$S_A^{(n)}(t) = \begin{cases} t \log(q_l^2) & t \leq r, \\ r \log(q_l^2) + (t - r) S_{\text{imp}}^{(n)} & t > r, \end{cases} \quad (14)$$

where $S_{\text{imp}}^{(n)}$ quantifies the operator entanglement [55] of the impurity gate, and is given by

$$e^{(1-n)S_{\text{imp}}^{(n)}} = \frac{1}{q_l^n q_r^n} \begin{array}{c} \square \\ \diagdown \quad \diagup \\ \square \end{array} \begin{array}{c} \circ \\ \diagdown \quad \diagup \\ \circ \end{array}. \quad (15)$$

This satisfies $0 \leq S_{\text{imp}}^{(n)} \leq \min\{\log(q_l^2), \log(q_r^2)\}$, where the lower bound is saturated by a purely reflecting impurity, i.e., $U(L, t) = \mathbb{1}$. The upper bound can be achieved by any gate acting as dual unitary on a $\min\{q_l^2, q_r^2\}$ -dimensional subspace and as the identity on the rest.

As an example, consider the case $q_l = q_r = q$ and $U(L, t) = \frac{1+icP}{1+ic}$, $c \in \mathbb{R}$, where P is the swap gate. With this choice we find

$$S_{\text{imp}}^{(n)} = \frac{1}{1-n} \log \left[\frac{q^2 - 1}{q^{2n}} \mathcal{T}^n + \left(\mathcal{R} + \frac{1}{q^2} \mathcal{T} \right)^n \right], \quad (16)$$

where $\mathcal{T} = c^2/(1+c^2)$, $\mathcal{R} = 1 - \mathcal{T}$ are the transmission and reflection coefficients of the impurity [56]. In the replica limit and for large q , the leading order term is

$$S_{\text{imp}} = \mathcal{T} \log(q^2) - \mathcal{T} \log \mathcal{T} - \mathcal{R} \log \mathcal{R}. \quad (17)$$

The result (14) is valid for any choice of bulk and impurity gates, integrable or chaotic. Accordingly, it can be interpreted using either the quasiparticle or entanglement membrane pictures. Within the quasiparticle picture, the change in entanglement growth at $t = r$ can be seen as arising from the fact that right-moving quasiparticles produced at points $L - 2r < x \leq L$ have had time to scatter off the impurity and enter the subsystem [56]. Prior to $t = r$ no quasiparticles have had the time to do so, hence the entanglement increases as in the pure case, where counter-propagating quasiparticle pairs generate maximal entanglement. In (17) we can interpret

the first term as this maximal entanglement rate reduced by the transmission coefficient. The last two terms are the entanglement entropy between the transmitted and reflected parts of a single quasiparticle that is split by the impurity, as previously discovered in integrable quantum impurity models [57–62]. Note that, the quasiparticle picture still applies despite the fact that the impurity generically breaks the integrability of the system [10, 11].

For chaotic models, the membrane picture is appropriate. In the pure case the tension of the membrane, calculated via the operator entanglement [31], is constant. Hence for $t \leq r$ the membrane takes any directed downward path emanating from the entangling point. When $t > r$, however, it is more energetically favorable for the membrane to travel along the impurity rather than the bulk since, not being dual unitary, it generates less entanglement. As a result, the optimal path consists of the membrane traveling to the impurity along the light cone until it reaches $x = L$ and then proceeding vertically down the impurity, see red dashed lines in Fig. 2. Inserting a projector onto the state \square — along the indicated path [16, 63] and computing the value of the resulting diagram we find (14), thus confirming the entanglement membrane picture. This is also in agreement with the value of the operator entanglement along the same path.

Finite subsystem—We now consider the case of a finite-size subsystem and restrict to the case where $r < \ell/2$, and also $\ell \ll L$ to avoid recurrences. In this case the dynamics can be split into a number of different regimes, the simplest to analyze being $t \leq \ell/2$. For that case the edges of the subsystem are not in causal contact with each other and $S_A^{(n)}(t)$ can be determined by summing up the contributions from each edge separately. These are obtained from (14) with $S_{\text{imp}}^{(n)} \rightarrow \log(q_l^2)$ for the edge farther from the impurity.

Beyond $t \geq \ell/2$ the effect of the finite subsystem size can be felt. Using the dual unitarity of the bulk we arrive at the following representation:

When $t \geq \ell + r$, this diagram can be further reduced using both the solvability of the initial state (1) and the unitarity of the local gates (9). The result is that

$$S_A^{(n)}(t \geq \ell + r) = \ell \log(q_l^2), \quad (19)$$

meaning that the subsystem relaxes to the infinite temperature state also in the presence of the impurity, although it is only guaranteed to do so at a much later time than that of a pure system, $t = \ell + r$ rather than $t = \ell/2$.

To investigate the intermediate times $\ell/2 < t < \ell + r$, however, it is necessary to examine some specific examples.

We start by considering the case where the circuit generates integrable dynamics, and in particular choose the simplest example where $U(x \neq L, t) = (u_+ \otimes u_-)P(v_+ \otimes v_-)$ with u_{\pm}, v_{\pm} being single-site unitaries (P is the swap gate). With this choice we can straightforwardly reduce (18) and find for $\ell/2 < t < \ell + r$ that

$$S_A^{(n)}(t) = \begin{cases} (\ell + r - t) \log(q_l^2) + (t - r) S_{\text{imp}}^{(n)} & t \leq \frac{\ell}{2} + r, \\ (t - r) \log(q_l^2) + (\ell + r - t) S_{\text{imp}}^{(n)} & \frac{\ell}{2} + r < t. \end{cases} \quad (20)$$

A notable feature of the above expression is that the entanglement decreases between $\ell/2 < t < \ell/2 + r$ and then increases again before saturating at $t = \ell + r$, see Fig. 1. We expect these features to be generic for integrable models as they admit an explanation via the quasiparticle picture [56]. In particular, the decrease in entanglement can be understood from the fact that the impurity can cause a quasiparticle to be reflected back inside the subsystem, thereby decreasing its overall contribution to the entanglement. After some time, however, the other quasiparticle of the pair will exit the subsystem from the other side and their contribution will be the same as in the pure case.

Thus $S_A^{(n)}(t)$ can exhibit non-monotonic behavior and a delayed saturation time for an integrable bulk circuit in the presence of an impurity. To investigate if these features can appear also in a non-integrable case, we introduce randomness to the bulk in the manner of [45] and also restrict to $n = 2$ and $q_l = q_r = q$. Upon averaging over different realizations, the bulk gates project onto the space spanned by the orthogonal states \circ — and \bullet — = $(q \circ$ — $- \circ$ —) / $\sqrt{q^2 - 1}$. Within this space the averaged gate takes a simple form [56, 64], depending only on q and on a parameter p , known as the entangling power of the gate [55, 64, 65]. This quantity, which we assume to be uniform among the bulk gates, obeys $0 \leq p \leq 1$ and determines the mixing properties of the bulk, i.e., the decay rate of dynamical correlations [66]. For $p = 0$ the averaged gate is the integrable swap gate, and light-cone correlations persist, while for $p = 1$ the decay rate is infinite.

We start by analyzing the case of $p = 1$ in the large q limit. There it can be shown that [56]

$$S_A^{(2)}(t) = \begin{cases} (t + r) \log(q^2) + (t - r) S_{\text{imp}}^{(2)} & t \leq t_*, \\ \ell \log(q^2) & t > t_*, \end{cases} \quad (21)$$

where $t_* \leq \ell - r$ is the saturation time, defined so that $S_A^{(2)}(t)$ is continuous. The upper bound for t_* occurs when the impurity is purely reflecting. Eq. (21) can be reproduced using the entanglement membrane picture. To see this, we note that in the early time regime $t \leq \ell/2$ the entanglement membrane follows the red dashed lines indicated in Fig. 2. On the other hand, for $t \geq \ell + r$

the exact result (19) suggests that the membrane instead runs horizontally across the subsystem, connecting the left and right edges. The expectation for the intermediate regime then would be that the membrane would continue to follow the path indicated in Fig. (2) until such time that the horizontal configuration is more favorable, in agreement with (21).

When the bulk does not have maximal entangling power, i.e. $0 < p < 1$, the picture changes. Once again we work in the large q limit such that $q \gg (1-p)^{-1}$. In the regime $\ell/2 < t \leq \ell/2 + r$ and after averaging, one can then show that the purity obeys the following lower bound [56],

$$\text{tr}[\rho_A^2(t)] \geq \frac{(1-p)^{\ell(2t-\ell)}}{q^{2\ell+2r-2t}} e^{(r-t)S_{\text{imp}}^{(2)}}. \quad (22)$$

At $t = \ell/2$ the lower bound agrees with the exact calculation, whereas for $\log[q^2(1-p)^{2\ell}] > S_{\text{imp}}^{(2)}$, the right-hand side increases with t , indicating that the entanglement entropy *must* decrease. At $p = 0$ the lower bound gives the exact result of (20), while for a dual unitary impurity the inequality is satisfied by the saturation value (19). Moreover, in the regime $\ell/2 + r < t < \ell + r$ we find

$$\text{tr}[\rho_A^2(t)] \geq \frac{1}{q^{2\ell}} + \frac{(1-p)^{2(\ell+r-t)(2t-\ell)}}{q^{2\ell}} \left(q^2 e^{-S_{\text{imp}}^{(2)}} - 1 \right)^{\ell+r-t}, \quad (23)$$

from which we can deduce that for $t < \ell + r$, $S_A^{(2)}(t)$ is still growing, at least until the second term in (23) becomes subleading in $1/q$ and can be omitted. Note that, at least to a leading order, the membrane picture is at odds with the possibility of decreasing entanglement due

to the basic properties of the entanglement membrane tension [15]. Thus, even though circuits with $0 < p < 1$ are generally chaotic (since integrable models only constitute a zero-measure subset [46]), their entanglement dynamics do not adhere to the membrane picture for a finite subsystem.

Conclusions— In this work we have examined the growth of bipartite entanglement in the presence of impurities in otherwise dual unitary quantum circuits. We have shown that for semi-infinite subsystems the exact result can be interpreted using either the quasiparticle or membrane pictures, while for finite-size subsystems the two theories give differing predictions. The impurity thus provides a way to probe the difference between chaotic and integrable dynamics of the entanglement entropy without the need for disjoint subsystems. Our work revealed a class of chaotic systems that do not obey the expected membrane picture, raising the need for the formulation of an intermediate theory interpolating between it and the quasiparticle picture (see [67] for recent work along these lines). Such an effort could be assisted by a systematic numerical study of the averaged random circuits we discussed. Another interesting continuation of this work would be to consider generalizations of these circuits to other gates in the dual unitary hierarchy [68] or charged dual unitary circuits [63].

Acknowledgements— The authors wish to thank B. Bertini, P. Calabrese, M. Goldstein, and K. Klobas for useful discussions. C.R. acknowledges support from ERC under Consolidator Grant number 771536 (NEMO) and the European Union - NextGenerationEU, in the framework of the PRIN Project HIGHEST number 2022SJCKAH.002. S.F. is grateful for the support of the Azrieli Foundation Fellows program and of the Tel-Aviv University Center for Nanoscience and Nanotechnology.

-
- [1] T. Giamarchi, *Quantum physics in one dimension*, International series of monographs on physics (Clarendon Press, Oxford, 2004).
 - [2] C. L. Kane and M. P. A. Fisher, Transport in a one-channel Luttinger liquid, *Phys. Rev. Lett.* **68**, 1220 (1992).
 - [3] L. F. Santos, Integrability of a disordered Heisenberg spin-1/2 chain, *Journal of Physics A: Mathematical and General* **37**, 4723 (2004).
 - [4] O. S. Barišić, P. Prelovšek, A. Metavitsiadis, and X. Zotos, Incoherent transport induced by a single static impurity in a Heisenberg chain, *Phys. Rev. B* **80**, 125118 (2009).
 - [5] E. J. Torres-Herrera and L. F. Santos, Local quenches with global effects in interacting quantum systems, *Phys. Rev. E* **89**, 062110 (2014).
 - [6] M. Žnidarič, Weak integrability breaking: Chaos with integrability signature in coherent diffusion, *Phys. Rev. Lett.* **125**, 180605 (2020).
 - [7] M. Pandey, P. W. Claeys, D. K. Campbell, A. Polkovnikov, and D. Sels, Adiabatic eigenstate deformations as a sensitive probe for quantum chaos, *Phys. Rev. X* **10**, 041017 (2020).
 - [8] M. Brenes, T. LeBlond, J. Goold, and M. Rigol, Eigenstate thermalization in a locally perturbed integrable system, *Phys. Rev. Lett.* **125**, 070605 (2020).
 - [9] M. Brenes, J. Goold, and M. Rigol, Low-frequency behavior of off-diagonal matrix elements in the integrable XXZ chain and in a locally perturbed quantum-chaotic XXZ chain, *Phys. Rev. B* **102**, 075127 (2020).
 - [10] F. Fritzsche and T. Prosen, Boundary chaos, *Phys. Rev. E* **106**, 014210 (2022).
 - [11] F. Fritzsche, R. Ghosh, and T. Prosen, Boundary chaos: Exact entanglement dynamics, *SciPost Phys.* **15**, 092 (2023).
 - [12] M. Brenes, E. Mascarenhas, M. Rigol, and J. Goold, High-temperature coherent transport in the XXZ chain in the presence of an impurity, *Phys. Rev. B* **98**, 235128 (2018).
 - [13] L. Amico, R. Fazio, A. Osterloh, and V. Vedral, Entanglement in many-body systems, *Rev. Mod. Phys.* **80**, 517 (2008).

- [14] P. Calabrese and J. Cardy, Evolution of entanglement entropy in one-dimensional systems, *Journal of Statistical Mechanics: Theory and Experiment* **2005**, P04010 (2005).
- [15] C. Jonay, D. A. Huse, and A. Nahum, Coarse-grained dynamics of operator and state entanglement (2018), [arXiv:1803.00089 \[cond-mat.stat-mech\]](https://arxiv.org/abs/1803.00089).
- [16] T. Zhou and A. Nahum, Entanglement membrane in chaotic many-body systems, *Phys. Rev. X* **10**, 031066 (2020).
- [17] V. Alba and P. Calabrese, Entanglement and thermodynamics after a quantum quench in integrable systems, *Proceedings of the National Academy of Sciences* **114**, 7947 (2017).
- [18] P. Calabrese, F. H. L. Essler, and M. Fagotti, Quantum quench in the transverse field Ising chain: I. time evolution of order parameter correlators, *Journal of Statistical Mechanics: Theory and Experiment* **2012**, P07016 (2012).
- [19] A. Coser, E. Tonni, and P. Calabrese, Entanglement negativity after a global quantum quench, *Journal of Statistical Mechanics: Theory and Experiment* **2014**, P12017 (2014).
- [20] V. Alba and P. Calabrese, Quantum information dynamics in multipartite integrable systems, *EPL (Europhysics Letters)* **126**, 60001 (2019).
- [21] D. X. Horváth and C. Rylands, Full counting statistics of charge in quenched quantum gases, *Phys. Rev. A* **109**, 043302 (2024).
- [22] B. Bertini, P. Calabrese, M. Collura, K. Klobas, and C. Rylands, Nonequilibrium full counting statistics and symmetry-resolved entanglement from space-time duality, *Phys. Rev. Lett.* **131**, 140401 (2023).
- [23] G. Perez, R. Bonsignori, and P. Calabrese, Quasiparticle dynamics of symmetry-resolved entanglement after a quench: Examples of conformal field theories and free fermions, *Phys. Rev. B* **103**, L041104 (2021).
- [24] G. Perez, R. Bonsignori, and P. Calabrese, Exact quench dynamics of symmetry resolved entanglement in a free fermion chain, *Journal of Statistical Mechanics: Theory and Experiment* **2021**, 093102 (2021).
- [25] J. Dubail, Entanglement scaling of operators: a conformal field theory approach, with a glimpse of simulability of long-time dynamics in 1+1d, *Journal of Physics A: Mathematical and Theoretical* **50**, 234001 (2017).
- [26] A. Rath, V. Vitale, S. Murciano, M. Votto, J. Dubail, R. Kueng, C. Branciard, P. Calabrese, and B. Vermersch, Entanglement barrier and its symmetry resolution: Theory and experimental observation, *PRX Quantum* **4**, 010318 (2023).
- [27] F. Ares, S. Murciano, and P. Calabrese, Entanglement asymmetry as a probe of symmetry breaking, *Nature Communications* **14**, 2036 (2023).
- [28] C. Rylands, K. Klobas, F. Ares, P. Calabrese, S. Murciano, and B. Bertini, Microscopic origin of the quantum mpemba effect in integrable systems, *Phys. Rev. Lett.* **133**, 010401 (2024).
- [29] B. Bertini, K. Klobas, M. Collura, P. Calabrese, and C. Rylands, Dynamics of charge fluctuations from asymmetric initial states, *Phys. Rev. B* **109**, 184312 (2024).
- [30] F. Rottoli, C. Rylands, and P. Calabrese, Entanglement Hamiltonians and the quasiparticle picture (2024), [arXiv:2407.01730 \[quant-ph\]](https://arxiv.org/abs/2407.01730).
- [31] M. A. Rampp, S. A. Rather, and P. W. Claeys, Entanglement membrane in exactly solvable lattice models, *Phys. Rev. Res.* **6**, 033271 (2024).
- [32] A. Foligno, P. Kos, and B. Bertini, Quantum information spreading in generalized dual-unitary circuits, *Phys. Rev. Lett.* **132**, 250402 (2024).
- [33] B. Bertini, K. Klobas, V. Alba, G. Lagnese, and P. Calabrese, Growth of Rényi entropies in interacting integrable models and the breakdown of the quasiparticle picture, *Phys. Rev. X* **12**, 031016 (2022).
- [34] A. Nahum, J. Ruhman, S. Vijay, and J. Haah, Quantum entanglement growth under random unitary dynamics, *Phys. Rev. X* **7**, 031016 (2017).
- [35] A. Foligno and B. Bertini, Entanglement of disjoint intervals in dual-unitary circuits: Exact results (2024), [arXiv:2408.16750 \[cond-mat.stat-mech\]](https://arxiv.org/abs/2408.16750).
- [36] V. Alba and P. Calabrese, Quantum information scrambling after a quantum quench, *Phys. Rev. B* **100**, 115150 (2019).
- [37] R. Modak, V. Alba, and P. Calabrese, Entanglement revivals as a probe of scrambling in finite quantum systems, *Journal of Statistical Mechanics: Theory and Experiment* **2020**, 083110 (2020).
- [38] B. Bertini, P. Kos, and T. Prosen, Exact spectral form factor in a minimal model of many-body quantum chaos, *Phys. Rev. Lett.* **121**, 264101 (2018).
- [39] S. Gopalakrishnan and A. Lamacraft, Unitary circuits of finite depth and infinite width from quantum channels, *Phys. Rev. B* **100**, 064309 (2019).
- [40] T. Prosen, Many-body quantum chaos and dual-unitarity round-a-face, *Chaos: An Interdisciplinary Journal of Nonlinear Science* **31**, 093101 (2021).
- [41] P. W. Claeys and A. Lamacraft, Ergodic and nonergodic dual-unitary quantum circuits with arbitrary local Hilbert space dimension, *Physical Review Letters* **126**, 100603 (2021).
- [42] P. Kos, B. Bertini, and T. Prosen, Correlations in perturbed dual-unitary circuits: Efficient path-integral formula, *Phys. Rev. X* **11**, 011022 (2021).
- [43] P. Kos and G. Styliaris, Circuits of space and time quantum channels, *Quantum* **7**, 1020 (2023).
- [44] A. Foligno, T. Zhou, and B. Bertini, Temporal entanglement in chaotic quantum circuits, *Phys. Rev. X* **13**, 041008 (2023).
- [45] B. Bertini and L. Piroli, Scrambling in random unitary circuits: Exact results, *Phys. Rev. B* **102**, 064305 (2020).
- [46] B. Bertini, P. Kos, and T. Prosen, Operator Entanglement in Local Quantum Circuits I: Chaotic Dual-Unitary Circuits, *SciPost Physics* **8**, 067 (2020).
- [47] B. Bertini, P. Kos, and T. Prosen, Operator Entanglement in Local Quantum Circuits II: Solitons in Chains of Qubits, *SciPost Phys.* **8**, 068 (2020).
- [48] T. Holden-Dye, L. Masanes, and A. Pal, Fundamental charges for dual-unitary circuits (2023), [arXiv:2312.14148 \[quant-ph\]](https://arxiv.org/abs/2312.14148).
- [49] M. Borsi and B. Pozsgay, Construction and the ergodicity properties of dual unitary quantum circuits, *Phys. Rev. B* **106**, 014302 (2022).
- [50] B. Bertini, P. Kos, and T. Prosen, Exact correlation functions for dual-unitary lattice models in 1 + 1 dimensions, *Phys. Rev. Lett.* **123**, 210601 (2019).
- [51] L. Piroli, B. Bertini, J. I. Cirac, and T. Prosen, Exact dynamics in dual-unitary quantum circuits, *Phys. Rev. B* **101**, 094304 (2020).
- [52] G. Giudice, G. Giudici, M. Sonner, J. Thoenniss,

- A. Lerose, D. A. Abanin, and L. Piroli, Temporal entanglement, quasiparticles, and the role of interactions, *Physical Review Letters* **128**, 220401 (2022).
- [53] E. Vernier, B. Bertini, G. Giudici, and L. Piroli, Integrable digital quantum simulation: Generalized Gibbs ensembles and Trotter transitions, *Physical Review Letters* **130**, 260401 (2023).
- [54] J. I. Cirac, D. Pérez-García, N. Schuch, and F. Verstraete, Matrix product states and projected entangled pair states: Concepts, symmetries, theorems, *Rev. Mod. Phys.* **93**, 045003 (2021).
- [55] S. A. Rather, S. Aravinda, and A. Lakshminarayan, Creating ensembles of dual unitary and maximally entangling quantum evolutions, *Physical Review Letters* **125**, 070501 (2020).
- [56] See the Supplemental Material for details on (i) Correlations across the impurity; (ii) The quasiparticle picture prediction for the entanglement entropy, broken down to contributions of quasiparticle pairs; (iii) Random gates with maximal entangling power, including the proof of (21); and (iv) Proofs of the bounds (22) and (23).
- [57] S. Fraenkel and M. Goldstein, Entanglement measures in a nonequilibrium steady state: Exact results in one dimension, *SciPost Phys.* **11**, 085 (2021).
- [58] S. Fraenkel and M. Goldstein, Extensive long-range entanglement in a nonequilibrium steady state, *SciPost Phys.* **15**, 134 (2023).
- [59] S. Fraenkel and M. Goldstein, Extensive long-range entanglement at finite temperatures from a nonequilibrium bias, *Phys. Rev. B* **110**, 035149 (2024).
- [60] S. Fraenkel and M. Goldstein, Exact asymptotics of long-range quantum correlations in a non-equilibrium steady state, *Journal of Statistical Mechanics: Theory and Experiment* **2024**, 033107 (2024).
- [61] L. Capizzi, S. Scopa, F. Rottoli, and P. Calabrese, Domain wall melting across a defect, *Europhysics Letters* **141**, 31002 (2023).
- [62] C. Rylands and P. Calabrese, Transport and entanglement across integrable impurities from generalized hydrodynamics, *Phys. Rev. Lett.* **131**, 156303 (2023).
- [63] A. Foligno, P. Calabrese, and B. Bertini, Nonequilibrium dynamics of charged dual-unitary circuits (2024), [arXiv:2407.21786](https://arxiv.org/abs/2407.21786).
- [64] A. Foligno and B. Bertini, Growth of entanglement of generic states under dual-unitary dynamics, *Physical Review B* **107**, 174311 (2023).
- [65] B. Jonnadula, P. Mandayam, K. Życzkowski, and A. Lakshminarayan, Entanglement measures of bipartite quantum gates and their thermalization under arbitrary interaction strength, *Physical Review Research* **2**, 043126 (2020).
- [66] S. Aravinda, S. A. Rather, and A. Lakshminarayan, From dual-unitary to quantum Bernoulli circuits: Role of the entangling power in constructing a quantum ergodic hierarchy, *Phys. Rev. Res.* **3**, 043034 (2021).
- [67] C. Jonay and T. Zhou, A physical theory of two-stage thermalization (2023), [arXiv:2310.04491](https://arxiv.org/abs/2310.04491) [quant-ph].
- [68] X.-H. Yu, Z. Wang, and P. Kos, Hierarchical generalization of dual unitarity, *Quantum* **8**, 1260 (2024).
- [69] P. Zanardi, Entanglement of quantum evolutions, *Phys. Rev. A* **63**, 040304 (2001).
- [70] M. A. Rampp, R. Moessner, and P. W. Claeys, From dual unitarity to generic quantum operator spreading, *Phys. Rev. Lett.* **130**, 130402 (2023).

Supplemental Material for “Entanglement in dual unitary quantum circuits with impurities”

Here we report some useful information complementing the main text. In particular:

- In Sec. I we discuss the correlation functions in the presence of the impurity and the transmission and reflection coefficients.
- In Sec. II we provide a quasiparticle-picture explanation for the entanglement dynamics of integrable circuits perturbed by an impurity.
- In Sec. III we present details of the entropy calculation for random gates with maximal entangling power.
- In Sec. IV we derive the bounds on the purity presented in the main text.

I. CORRELATIONS

For pure dual unitary brickwork quantum circuits, it has been shown that correlation functions are non-trivial only between points connected by light rays [50]. When some of the gates are perturbed from dual unitarity, however, this special structure is lost and correlation functions involve sums over all allowed paths through the system [42]. For the particular system we study, the situation is much simpler. Infinite temperature correlations can occur only between points connected along light rays or those which are connected by a ray that reflects off the impurity, see Fig. SM-1.

It is instructive to see this in action for a specific choice of an impurity gate. We take $q_l = q_r = q$ and choose

$$U(L, t) = \frac{\mathbb{1} + icP}{1 + ic}, \quad (\text{SM-1})$$

where $c \in \mathbb{R}$ and P is the swap gate on two qudits, which acts as $P|ij\rangle = |ji\rangle$. The form of this impurity gate is quite natural as it tunes between a completely reflecting impurity at $c = 0$, which does not allow for the transmission of information, and a completely transparent one at $c \rightarrow \infty$, which is dual unitary.

Let us consider the infinite temperature 2-point correlation function $\mathcal{C}^{\alpha,\beta}(x, y; t) \equiv \text{tr}[\sigma^\alpha(x, t)\sigma^\beta(y, 0)]$, where $\sigma^{\alpha,\beta}(z, \tau)$ are traceless single-site operators at space-time positions z, τ . Setting $y \geq L + 1$ with $y - L$ being odd, the computation of this quantity can be reduced to the diagrams in Fig. SM-1 (a) and (b), where it is understood that there is only a single replica, $n = 1$. Using (SM-1) we find that

$$\mathcal{C}^{\alpha,\beta}(y - 2t, y; t) = \mathcal{T} \lim_{c \rightarrow \infty} \mathcal{C}^{\alpha,\beta}(y - 2t, y; t), \quad (\text{SM-2})$$

$$\mathcal{C}^{\alpha,\beta}(2t - y + 2L + 1, y; t) = \mathcal{R} \lim_{c \rightarrow \infty} \mathcal{C}^{\alpha,\beta}(y - 2t, y; t), \quad (\text{SM-3})$$

where $\mathcal{T} = \frac{c^2}{1+c^2}$, $\mathcal{R} = 1 - \mathcal{T}$ are the transmission and reflection coefficients for the impurity. These multiply a factor that corresponds to the correlation function in the presence of a completely transparent impurity. Thus, irrespective of the nature of the bulk, information can be transmitted or reflected from the impurity. The same coefficients then appear in the entanglement entropy in Eq. (16) of the main text. For the case of a quench, the correlation functions can no longer be reduced to this simple form due to the impurity not being dual unitary, see Fig. SM-1 (c) and (d). As a result, they depend on higher powers of \mathcal{T} and \mathcal{R} , indicating that multiple scattering processes are involved.

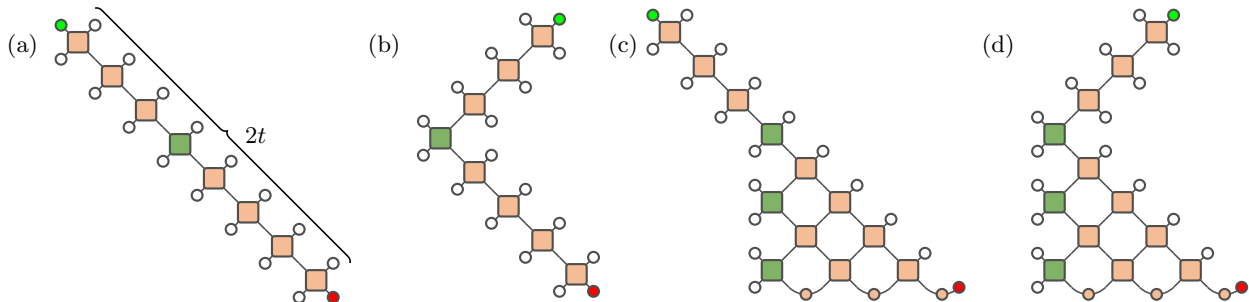


FIG. SM-1. (a,b) Diagrammatic representation of infinite temperature correlation functions $\text{tr}[\sigma^\alpha(x, t)\sigma^\beta(y, 0)]$ in the presence of an impurity. Operators σ^β , σ^α are denoted by red and green circles, respectively, and the local gates correspond to the single replica case $n = 1$. Correlation functions are supported along (a) light rays between points or (b) rays that reflect off the impurity. Depicted is the case of $t = 4$, $y = L + 5$, and (a) $x = L - 3$ or (b) $x = L + 4$. (c,d) Correlation functions after a quench for the same parameters.

II. QUASIPARTICLE PICTURE OF ENTANGLEMENT DYNAMICS

In this section, we explain how the results in Eqs. (14) and (20) of the main text, which state the entanglement entropy evolution in an integrable circuit perturbed by an impurity, are captured by a coarse-grained quasiparticle picture description. In particular, we examine entanglement dynamics ensuing from pairs of maximally-entangled counter-propagating quasiparticles generated uniformly across the system at $t = 0$. To match the circuit defined in the main text, their density is such that a single pair is generated in any interval of length $\Delta x = 2$, and the quasiparticle velocity is $v = 2$. The quasiparticles propagate independently almost everywhere, and can interact only at the location of the impurity, $x = L$.

Therefore, to obtain a quasiparticle picture description, one must determine the effect of the impurity on the entanglement between quasiparticles. Consider a quasiparticle pair generated at a point $x = x_0 < L$ to the left of the impurity, and let $A_{x_0}^{(+)}$ and $A_{x_0}^{(-)}$ denote the single-quasiparticle subsystems of the right-moving and left-moving parts of the pair, respectively. At time $t = (L - x_0)/v$, the right-moving quasiparticle reaches the impurity, simultaneously with the left-moving quasiparticle of the pair generated at $x = 2L - x_0$, and they are both reflected off the impurity. The two quasiparticle pairs become entangled due to the impurity, the action of which corresponds to the unitary $U(L, t)$. By the definition of operator entanglement [69, 70], we then have that the entropy of the combined subsystem $A_{x_0}^{(+)} \cup A_{x_0}^{(-)}$ is

$$S_{A_{x_0}^{(+)} \cup A_{x_0}^{(-)}}^{(n)} = S_{\text{imp}}^{(n)}, \quad (\text{SM-4})$$

where $S_{\text{imp}}^{(n)}$ was defined in Eq. (15) of the main text. That is, the two *pairs* on the opposite sides of the impurity are entangled to each other to an extent determined by $S_{\text{imp}}^{(n)}$.

Therefore, if a subsystem A contains at some point t in time the two quasiparticles generated at $x = x_0$, their contribution to its entropy $S_A^{(n)}$ will be $\Delta S_A^{(n)} = 0$ for $t < (L - x_0)/v$ and $\Delta S_A^{(n)} = S_{\text{imp}}^{(n)}$ for $t > (L - x_0)/v$. If A contains only one of these quasiparticles, at any point in time its contribution to $S_A^{(n)}$ will be maximal, i.e., $\Delta S_A^{(n)} = \log(q_l)$. This is clear if the quasiparticle in question is the left one (which never interacts with another quasiparticle), or the right one for $t < (L - x_0)/v$. The fact that it is true also for the right quasiparticle when $t > (L - x_0)/v$ is observed by noting that the two quasiparticles that meet at the impurity constitute a subsystem with maximal entropy; since the impurity operator $U(L, t)$ cannot reduce this entropy, they maintain their maximal entropy, meaning that each one of them must be maximally entangled to the rest of the system. A schematic example for the entropy contribution of a single quasiparticle pair is depicted in Fig. SM-2.

What remains now is to add up the contributions of pairs generated at $t = 0$ across the system. Our computation for a single pair implies that we should take into account only pairs generated at positions $x < L$, since their independent contributions already take into account the interactions with pairs generated at positions $x > L$. We divide the domain $x < L$ into four regions, as shown in Fig. SM-2. For pairs generated in Region I, that is, the region $(0, L - 2\ell - 2r)$ outside A , only their right-moving part can be found inside A , with maximal entanglement contribution. The entanglement entropy arising from quasiparticles generated in this region is therefore

$$S_A^{(n, \text{I})}(t) = \begin{cases} t \log(q_l) & 0 \leq t < \ell, \\ \ell \log(q_l) & \ell \leq t < \ell + 2r, \\ (t - 2r) \log(q_l) & \ell + 2r \leq t < 2\ell + 2r, \\ 2\ell \log(q_l) & 2\ell + 2r \leq t. \end{cases} \quad (\text{SM-5})$$

For pairs generated in Region II, defined as $(L - 2\ell - 2r, L - \ell)$, it is easy to check that the two quasiparticles of the same pair can be inside A simultaneously only before the right-moving one exits A for the first time, so they have a nonzero contribution to $S_A^{(n)}$ only when A contains just one of them. This yields the contribution

$$S_A^{(n, \text{II})}(t) = \begin{cases} t \log(q_l) & 0 \leq t < \frac{\ell}{2} - r, \\ (2t + r - \frac{\ell}{2}) \log(q_l) & \frac{\ell}{2} - r \leq t < \frac{\ell}{2}, \\ (\frac{3}{2}\ell + r - 2t) \log(q_l) & \frac{\ell}{2} \leq t < \frac{\ell}{2} + r, \\ (\frac{\ell}{2} - r) \log(q_l) & \frac{\ell}{2} + r \leq t < \ell, \\ (t - \frac{\ell}{2} - r) \log(q_l) & \ell \leq t < \ell + 2r, \\ (\frac{\ell}{2} + r) \log(q_l) & \ell + 2r \leq t < \frac{3}{2}\ell + r, \\ (2\ell + 2r - t) \log(q_l) & \frac{3}{2}\ell + r \leq t < 2\ell + 2r, \\ 0 & 2\ell + 2r \leq t. \end{cases} \quad (\text{SM-6})$$

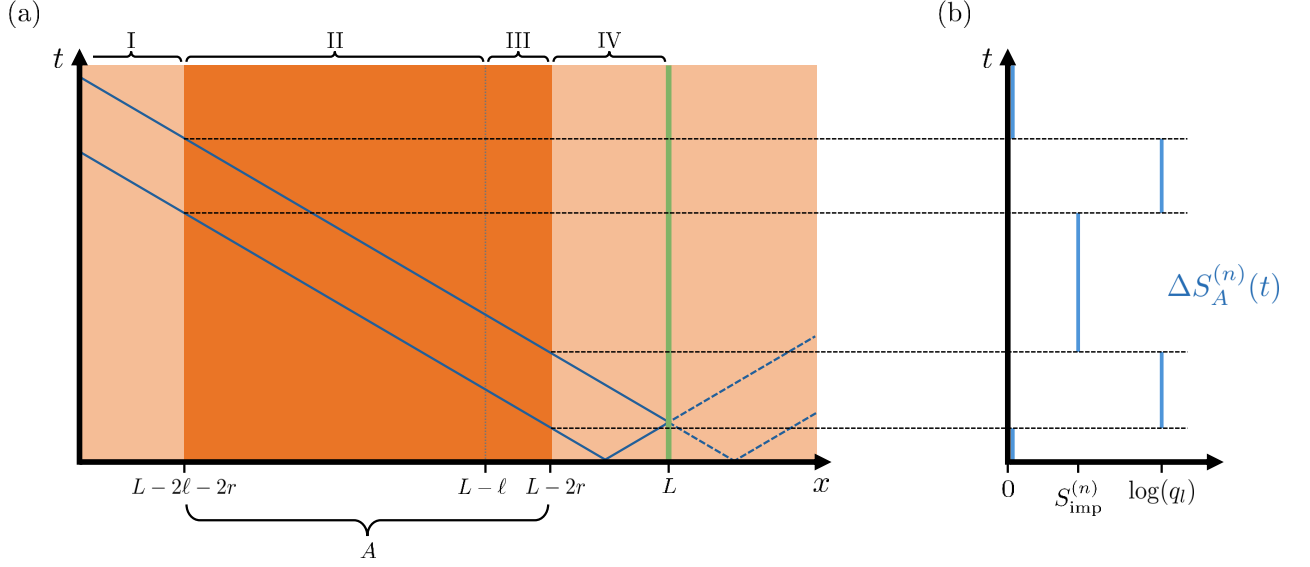


FIG. SM-2. The quasiparticle picture of entanglement dynamics in the presence of an impurity. (a) Coarse-grained space-time plot of the system, with an example for a pair of correlated counter-propagating particles generated at $t = 0$ on the left side of the impurity (solid blue lines); at a certain point in time, the right-moving quasiparticle reaches the impurity at $x = L$ (solid vertical line), and becomes entangled with a quasiparticle from a pair generated on the right side of the impurity (dashed blue lines); then both quasiparticles are reflected off the impurity. The plot also shows the location of the finite subsystem A defined in the main text, and the division of the domain to the left of the impurity into the four regions discussed in Sec. II. (b) The contribution to the entanglement entropy of A arising from the exemplary quasiparticle pair as a function of time.

In contrast to the cases of Regions I and II, quasiparticles of the same pair generated in $(L-l, L)$ can, during a certain time span, be simultaneously inside A even after the right quasiparticle is reflected off the impurity, contributing $S_{\text{imp}}^{(n)}$ to $S_A^{(n)}$ during that time. Adding up contributions from quasiparticles generated in Region III, namely the region $(L-l, L-2r)$ contained in A , and in Region IV, namely the region $(L-2r, L)$ between A and the impurity, one obtains the following:

$$S_A^{(n, \text{III})}(t) = \begin{cases} t \log(q_l) & 0 \leq t < \min\{\frac{\ell}{2} - r, 2r\}, \\ \min\{\frac{\ell}{2} - r, 2r\} \log(q_l) + \max\{t - 2r, 0\} S_{\text{imp}}^{(n)} & \min\{\frac{\ell}{2} - r, 2r\} \leq t < \max\{\frac{\ell}{2} - r, 2r\}, \\ (\frac{\ell}{2} + r - t) \log(q_l) + (t - 2r) S_{\text{imp}}^{(n)} & \max\{\frac{\ell}{2} - r, 2r\} \leq t < \frac{\ell}{2} + r, \\ (t - \frac{\ell}{2} - r) \log(q_l) + (\ell - t) S_{\text{imp}}^{(n)} & \frac{\ell}{2} + r \leq t < \ell, \\ (\frac{\ell}{2} - r) \log(q_l) & \ell \leq t < \ell + 2r, \\ (\frac{3}{2}\ell + r - t) \log(q_l) & \ell + 2r \leq t < \frac{3}{2}\ell + r, \\ 0 & \frac{3}{2}\ell + r \leq t, \end{cases} \quad (\text{SM-7})$$

and

$$S_A^{(n, \text{IV})}(t) = \begin{cases} t \log(q_l) & 0 \leq t < r, \\ (2r - t) \log(q_l) + (t - r) S_{\text{imp}}^{(n)} & r \leq t < 2r, \\ r S_{\text{imp}}^{(n)} & 2r \leq t < \ell, \\ (t - \ell) \log(q_l) + (\ell + r - t) S_{\text{imp}}^{(n)} & \ell \leq t < \ell + r, \\ (\ell + 2r - t) \log(q_l) & \ell + r \leq t < \ell + 2r, \\ 0 & \ell + 2r \leq t. \end{cases} \quad (\text{SM-8})$$

Finally, the total entanglement entropy of A is obtained from summing up the contributions arising from the

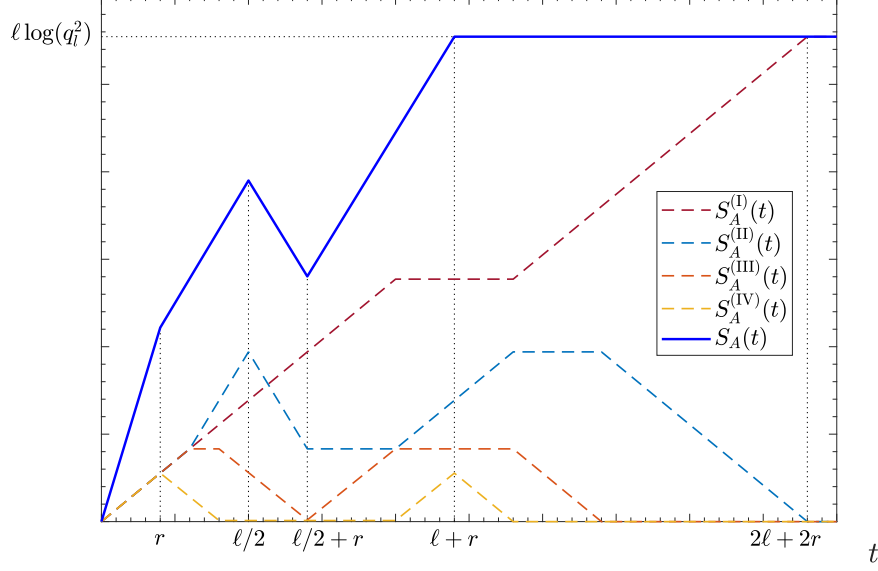


FIG. SM-3. Entanglement entropy dynamics in the bulk swap-gate circuit perturbed by an impurity. Subsystem A has length 2ℓ and is a distance $2r$ from the impurity. Results are shown for local Hilbert space dimension $q_l = 2$ and the impurity given in Eq. (16) of the main text, with $c = 0.05$, in the replica limit $n \rightarrow 1$. The plot shows the contributions arising from Regions I-IV (Eqs. (SM-5)–(SM-8)) as well as the total entropy (Eq. (SM-9)).

different regions. This leads to

$$S_A^{(n)}(t) = S_A^{(n,I)}(t) + S_A^{(n,II)}(t) + S_A^{(n,III)}(t) + S_A^{(n,IV)}(t) = \begin{cases} 2t \log(q_l^2) & 0 \leq t < r, \\ (t+r) \log(q_l^2) + (t-r) S_{\text{imp}}^{(n)} & r \leq t < \frac{\ell}{2}, \\ (\ell+r-t) \log(q_l^2) + (t-r) S_{\text{imp}}^{(n)} & \frac{\ell}{2} \leq t < \frac{\ell}{2} + r, \\ (t-r) \log(q_l^2) + (\ell+r-t) S_{\text{imp}}^{(n)} & \frac{\ell}{2} + r \leq t < \ell + r, \\ \ell \log(q_l^2) & \ell + r \leq t, \end{cases} \quad (\text{SM-9})$$

which indeed fits the result for the swap-gate circuit presented in the main text, see Eqs. (14) and (20). Fig. SM-3 shows the same example that appeared in Fig. 1 of the main text of the entanglement entropy dynamics predicted by the quasiparticle picture, along with the different contributions arising from Regions I-IV.

III. ENTANGLEMENT EVOLUTION FOR RANDOM GATES WITH MAXIMAL ENTANGLING POWER

In this section, we detail the exact calculation of the second Rényi entanglement entropy evolution for random dual unitary bulk gates with maximal entangling power, $p = 1$, in the large q limit. The entangling power of a bulk gate U is defined as

$$p = \frac{1}{q^2(q^2-1)} \left(q^4 - \text{tr} \left[\left(\tilde{U}^{\text{T}_2} (\tilde{U}^{\text{T}_2})^\dagger \right)^2 \right] \right), \quad (\text{SM-10})$$

where T_2 represents the partial transpose with respect to the second qudit on which \tilde{U} acts. Upon averaging, the bulk gate assumes a simple form, written in terms of q and p . Indeed, with respect to the orthogonal basis $\{\circ, \bullet\}$ of the subspace onto which the gate is projected, it can be represented in the following matrix form (assuming $q \gg 1$) [64]:

$$\square \approx \begin{pmatrix} 1 & 0 & 0 & 0 \\ 0 & 0 & 1-p & p/q \\ 0 & 1-p & 0 & p/q \\ 0 & p/q & p/q & 1 \end{pmatrix}. \quad (\text{SM-11})$$

We now substitute $p = 1$ and proceed to prove Eq. (21) of the main text. We will use the fact that $\square - \approx \bullet - + \circ - / q$ for $q \gg 1$.

Two main properties of the averaged gates that will be used in the calculation are

$$\text{Diagram of } m \text{ gates} \approx \frac{1}{q^m} \text{Diagram of } \square \otimes \left[\begin{array}{c} \bullet \\ \square \end{array} \right]^{\otimes m}, \quad (\text{SM-12})$$

which immediately stems from the form of the averaged gate in (SM-11) for $p = 1$, and

$$\text{Diagram of } m \text{ gates} \approx \left[\square \right]^{\otimes m} \otimes \square - \frac{1}{q^2} \left[\square \right]^{\otimes (m-1)} \otimes \square \otimes \square, \quad (\text{SM-13})$$

which holds to a leading order in $1/q$, and may be straightforwardly proved by induction. Eqs. (SM-12) and (SM-13) should be interpreted so that when the $m + 1$ free legs of the two diagrams on the two sides of an equation are connected to the $m + 1$ free legs of an arbitrary diagram, they yield the same result at the leading order in $1/q$.

We focus on the non-universal time regime $\ell/2 < t < \ell + r$ (recall that outside this regime the results are independent of the bulk gates), and begin with the earlier regime $\ell/2 < t \leq \ell/2 + r$. Applying the decomposition $\text{Diagram of } \square \otimes \square = (\text{Diagram of } \square \otimes \square + \text{Diagram of } \bullet \bullet) / q^4$ to the leftmost edge of the purity diagram, and using the properties in (SM-12) and (SM-13), we see that

$$\begin{aligned} \text{tr}[\rho_A^2(t)] &= \text{Diagram of } \ell \text{ and } 2r \text{ gates} \times q^{\ell+2r-6t} \\ &\approx \text{Diagram of } \ell-1 \text{ gates} \times q^{\ell+2r-6t-3} + \text{Diagram of } \ell-2 \text{ gates} \times q^{2\ell+2r-8t-4} \\ &\quad - \text{Diagram of } \ell-2 \text{ gates} \times q^{2\ell+2r-8t-6}, \end{aligned} \quad (\text{SM-14})$$

which reduces to

$$\begin{aligned}
 \text{tr}[\rho_A^2(t)] \approx & \left(\text{Diagram 1} \right) \times q^{\ell+2r-6t-3} + \left(\text{Diagram 2} \right)^{t-r} \times q^{2r-6t} \\
 & - \left(\text{Diagram 3} \right) \times q^{\ell+2r-6t-6}. \tag{SM-15}
 \end{aligned}$$

We now show that the last term in (SM-15) (with the negative sign) is subleading in $1/q$ compared to the first two. Indeed, in this last term, we resolve the initial state at the leftmost edge of the diagram as before, and upper-bound the contribution of the diagram with \bullet by replacing these states with \square . By doing so repeatedly until the diagram is completely reduced, we find that

$$\left(\text{Diagram 3} \right) \times q^{\ell+2r-6t-6} \leq \frac{1}{q^{4t}} + \left(\text{Diagram 4} \right)^{t-r} \times q^{2r-6t-4}. \tag{SM-16}$$

In contrast, the first term in (SM-15) can be lower-bounded as

$$\left(\text{Diagram 1} \right) \times q^{\ell+2r-6t-3} \geq \frac{1}{q^{2\ell}}, \tag{SM-17}$$

by resolving the initial state and keeping only the contributions of \circ states. Given that $t > \ell/2$, the last term of (SM-15) is thus upper-bounded by an expression that is subleading in $1/q$ compared to the first two terms, meaning that we may omit it and write

$$\text{tr}[\rho_A^2(t)] \approx \left(\text{Diagram 1} \right) \times \frac{1}{q^{6t-\ell-2r+3}} + \frac{1}{q^{6t-2r}} \left(\text{Diagram 2} \right)^{t-r}. \tag{SM-18}$$

Finally, we may apply this rule repeatedly to reduce the remaining diagram, obtaining

$$\text{tr}[\rho_A^2(t)] \approx \frac{1}{q^{2\ell}} + \frac{1}{q^{2t+2r}} e^{(r-t)S_{\text{imp}}^{(2)}}. \tag{SM-19}$$

An analogous treatment of the later non-universal time regime, namely $\ell/2 + r < t < \ell + r$, yields the exact same form of the purity as in (SM-19).

The result of (SM-19) should be interpreted like so: the exact expression for the purity contains two terms, but almost for any t one of the terms dominates the other to a leading order in $1/q$, such that the contribution of the subleading term of the two may be neglected. We can define the time t_* as that at which the two terms are comparable,

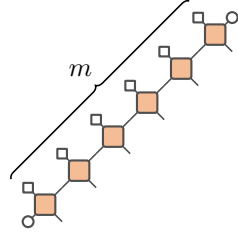
$$\frac{1}{q^{2\ell}} \approx \frac{1}{q^{2t_*+2r}} e^{(r-t_*)S_{\text{imp}}^{(2)}}, \quad (\text{SM-20})$$

and then the evolution of the second Rényi entropy is given by Eq. (21) of the main text.

IV. PROOF OF BOUNDS IN THE NON-UNIVERSAL TIME REGIME

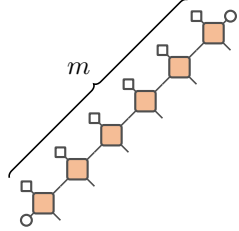
In this section, we prove two lower bounds to the purity of $\rho_A(t)$ in the non-universal time regime $\ell/2 < t < \ell + r$, for averaged random dual unitary bulk gates with a uniform entangling power $p < 1$ and assuming a large local Hilbert dimension, $q \gg (1-p)^{-1}$. The first bound, appearing in Eq. (22) of the main text, applies in the earlier time regime $\ell/2 < t \leq \ell/2 + r$, while the second bound, appearing in Eq. (23) of the main text, applies in the later time regime $\ell/2 + r < t < \ell + r$. In the derivation that follows, we use the matrix form of the averaged gate given in (SM-11).

In order to prove the first bound, we first note that, for any integer m ,



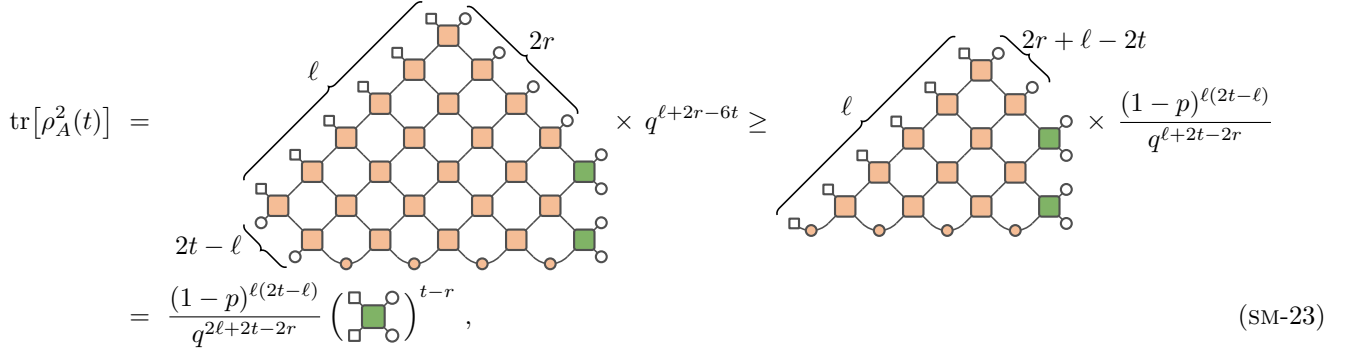
$$\approx q^2 \left[(1-p) \begin{array}{c} \bullet \\ \bullet \end{array} + \frac{1}{q} \begin{array}{c} \circ \\ \circ \end{array} \right]^{\otimes m}. \quad (\text{SM-21})$$

This can be seen by writing $\square \approx \bullet + \circ/q$, and noting that whenever the operation $\begin{array}{c} \circ \\ \square \\ \bullet \end{array} \approx (1-p) \begin{array}{c} \bullet \\ \bullet \end{array} + p/q \begin{array}{c} \bullet \\ \circ \end{array}$ is encountered while reducing the diagram, the second term on the right-hand side can be omitted as it produces only a subleading contribution in $1/q$. From (SM-21) one can readily see that



$$\geq q^2 (1-p)^m [\square]^{\otimes m}. \quad (\text{SM-22})$$

As before, one should interpret the inequality as pertaining to the values of an arbitrary diagram with m free legs after it is contracted with either of the two diagrams above. Next, we apply (SM-22) to the diagram that stands for the purity at a time $\ell/2 < t \leq \ell/2 + r$, and observe that



$$\begin{aligned} \text{tr}[\rho_A^2(t)] &= \text{Diagram} \times q^{\ell+2r-6t} \geq \text{Diagram} \times \frac{(1-p)^{\ell(2t-\ell)}}{q^{\ell+2t-2r}} \\ &= \frac{(1-p)^{\ell(2t-\ell)}}{q^{2\ell+2t-2r}} \left(\begin{array}{c} \square \\ \square \\ \circ \end{array} \right)^{t-r}, \end{aligned} \quad (\text{SM-23})$$

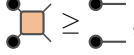
which proves the first bound, given in Eq. (22) of the main text.

To prove the second bound, we will repeatedly use the decomposition $\circ\text{---}\circ = (\circ\text{---}\circ + \bullet\text{---}\bullet)/q^4$ of the initial state to reduce the purity diagram for $\ell/2 + r < t < \ell + r$. The first step leads to

$$\begin{aligned}
 \text{tr}[\rho_A^2(t)] &= \text{Diagram}(\ell, 2r, 2t-\ell) \times q^{\ell+2r-6t} \\
 &= \text{Diagram}(\ell, 2r, 2t-\ell) \times q^{\ell+2r-6t-4} + \text{Diagram}(\ell, 2r, 2t-\ell, \bullet\text{---}\bullet) \times q^{\ell+2r-6t-4},
 \end{aligned}
 \tag{SM-24}$$

which, by using the fact that $\circ\text{---}\circ \geq (1-p)\bullet\text{---}\bullet$, yields

$$\begin{aligned}
 \text{tr}[\rho_A^2(t)] &\geq \text{Diagram}(\ell-1, 2r, 2t-\ell+1) \times q^{\ell+2r-6t-3} + \text{Diagram}(\ell, 2r, 2t-\ell, \bullet\text{---}\bullet) \times \frac{(1-p)^{2t-\ell}}{q^{6t+2-\ell-2r}}.
 \end{aligned}
 \tag{SM-25}$$

By also using the fact that , we eventually arrive at the result

$$\begin{aligned}
\text{tr}[\rho_A^2(t)] &\geq \text{Diagram 1} \times \frac{1}{q^{3t+2\ell+r}} + \text{Diagram 2} \times \frac{(1-p)^{(2t-\ell)(\ell+r-t)}}{q^{4t+\ell}} \\
&= \frac{1}{q^{2\ell}} + \text{Diagram 3} \times \frac{(1-p)^{(2t-\ell)(\ell+r-t)}}{q^{4t+\ell}}. \tag{SM-26}
\end{aligned}$$

The diagrams are as follows: Diagram 1 is a large grid with orange squares and white circles, with some squares turned green. Diagram 2 is similar but has a dashed line at the bottom right labeled $\ell+r-t$ pointing to a specific configuration. Diagram 3 is identical to Diagram 1 but with a different boundary configuration at the bottom right.

By inserting the completeness relation $\mathbb{1} = (\text{circle with slash} + \text{two dots})/q^2$ into legs of impurity gates, we then find that

$$\begin{aligned}
\text{tr}[\rho_A^2(t)] &\geq \frac{1}{q^{2\ell}} + \text{Diagram 4} \times \left(\frac{1}{q^2} \text{Diagram 5}\right)^{\ell+r-t} \times \frac{(1-p)^{(\ell+r-t)(2t-\ell)}}{q^{4t+\ell}} \\
&\geq \frac{1}{q^{2\ell}} + \frac{(1-p)^{2(\ell+r-t)(2t-\ell)}}{q^{2\ell}} \times \left(\frac{1}{q^2} \text{Diagram 6} - 1\right)^{\ell+r-t}, \tag{SM-27}
\end{aligned}$$

Diagram 4 is a grid similar to the previous ones but with a different boundary. Diagram 5 is a square with a dot on its top-left corner. Diagram 6 is a square with a dot on its top-left corner and a slash on its top edge.

where in the last inequality we again used the bound $\text{Diagram 6} \geq (1-p) \text{Diagram 7}$. This proves the bound given in Eq. (23) of the main text.